ChemPubSoc Europe

DOI: 10.1002/celc.201700955

CHEMELECTROCHEM Articles

# Bifunctional Electrocatalysts ($Co_9S_8$@NSC) Derived from a Polymer–Metal Complex for the Oxygen Reduction and Oxygen Evolution Reactions

Saad M Alshehri,[a] Jahangeer Ahmed,[a] Aslam Khan,[b] Mu Naushad,[a] and Tansir Ahamad*[a]

Bifunctional catalysts for water electrolysis are important for renewable and clean energy transformation processes like fuel cells, lithium–oxygen batteries, and so forth. Despite tremendous efforts, developing efficient bifunctional electrocatalysts with low cost and long-term durability remains a great challenge. Herein, the synthesis of $Co_9S_8$ nanocrystals encapsulated in nitrogen/sulfur-doped mesoporous graphitized carbon derived from a polymer–metal complex is reported, which exhibit similar electrocatalytic activity and superior stability for water-splitting reactions (oxygen reduction/oxygen evolution). The remarkable electrochemical properties are mainly attributed to the synergetic effects between $Co_9S_8$, heteroatoms and graphitized carbon in alkaline medium, especially for the oxygen evolution reaction. The present strategy to fabricate $Co_9S_8$ nanocrystals in nitrogen and sulfur doped carbon using a single-source precursor offers many prospects in developing highly effective electrocatalysts in rechargeable metal–air batteries.

## 1. Introduction

Growing the demand of global energy and the crisis of traditional nonrenewable fuel are encouraging the research for alternative energy sources such as fuel cells, air-batteries and metal – oxygen batteries with high efficiency and low cost.[1] Electrolysis of water (ORR/OER) is an outstanding technology in demand for the production of clean power without the emission of greenhouse gases. However, the efficiency of water electrolysis is limited due to the required large overpotential above the standard reaction potential (1.23 V). To minimize the overpotential at both electrodes and using electricity derived from wind and solar power to split water is a challenging task.[2] The efficiency of water electrolysis strongly depends on the composition and nature of electrocatalyst. Up to now, Pt, Ru, Ir and other precious metal-based materials have been found to be effective bifunctional catalysts toward the splitting of water (ORR/OER).[3] However, their comprehensive uses as commercial electrocatalyst are limited due to their prohibitive cost and paucity in globe.

Therefore, it is still a challenging task to develop low-cost efficient bifunctional catalysts with long-term durability for electrolytic splitting of water (ORR and OER) to replace conventional precious metals.[4] On the other hand, cobalt is an abundant metal; some of the cobalt oxide ($CoO_x$), cobalt sulfide ($CoS_x$), and cobalt based nanocomposites have recently been reported to show bifunctional electrocatalytic performances.[5] Based on cost, performance, stability, and safety issues, cobalt sulfides (CoS, $CoS_2$, $Co_2S_3$, $Co_3S_4$ and $Co_9S_8$) are very attractive for electrochemical applications compared to cobalt and other metal oxides.[5b,6] Among these cobalt sulfides, cobalt-rich sulfide ($Co_9S_8$) has fascinated researchers because of its attractive applications like hydro desulfurization. However, to use of pure $Co_9S_8$ nanoparticles for bifunctional catalytic performances are still far because of their small specific surface area, insufficient conductivity, easy aggregation of nanoparticles, poor stability in basic medium and the intrinsic lack of active sites. The main hurdle to their use as a bifunctional electrocatalyst for overall water splitting is that the $Co_9S_8$ nanoparticles are easily oxidized in alkaline solution by which their electrical conductivity as well as their long term durability also decreased.[7] One effective way to improve the performance as well as the stability of $Co_9S_8$, expand and improve their applications is to hybridize them with conducting carbon and carbon based materials such as carbon nanotubes/graphene.[8] These materials do not improve the conductivity of $Co_9S_8$ only but also they improve the catalytic activity as well as stability due to the redox cycling nature of carbon atoms and leading to reduced ORR potential. Furthermore, the doping of heteroatoms (N, O and S) into carbon based materials could efficiently create the active sites due to high positive charge density that induced charge transfer from adjacent carbon atoms and also change the mode of $O_2$ adsorption that weaken the O–O bonding for efficient ORR.[5b,9] Nevertheless, it remains very challenging to develop a single effective catalyst by taking all the above ideas in the cost and performance effective manner.

To the best of our knowledge, the synthesis of $Co_9S_8$ nanoparticles encapsulated in nitrogen–sulfur doped graphitized carbon using single source precursor (polymer metal complexes) and its bifunctional catalytic activity for electrolysis

[a] Prof. S. M. Alshehri, Dr. J. Ahmed, Dr. M. Naushad, Dr. T. Ahamad
Department of Chemistry
King Saud University
Riyadh, Kingdom of Saudi Arabia
E-mail: tahamed@ksu.edu.sa
[b] Dr. A. Khan
King Abdullah Institute for Nanotechnology
King Saud University
Riyadh, Kingdom of Saudi Arabia

Supporting information for this article is available on the WWW under https://doi.org/10.1002/celc.201700955

of water has not been explored yet. Herein, we have successfully synthesized $Co_9S_8$@NSC nanocomposites using a phenylthiourea formaldehyde cobalt complex as a single source precursor, these materials acts as an efficient bifunctional electrocatalyst for both ORR and OER with good durability in alkaline environments.

## Experimental Section

### Preparation of the Electrocatalyst

The polymeric ligand (phenylthiourea formaldehyde) and the polymer cobalt complex are prepared using our previous reported method.[10] The polymer cobalt complex [PTF–Co(II)] is used as the precursor for the fabrication of $Co_9S_8$@NSC nanocomposites. The $Co_9S_8$@NSC nanocomposites are synthesized by a simple thermal treatment of PTF–Co(II), containing abundant C, N, S and Co atoms at 600–900 °C in He (helium) atmosphere. The accessible Co nanoparticles and other metal impurities is washed using 10 wt% HCl and followed by adequate washing with distilled water and dry in vacuum oven to obtained $Co_9S_8$@NSC nanocomposites.

### Characterization of the Electrocatalyst

Characterization of the materials was carried out using Raman spectroscopy, Transmission electron microscopy (TEM), X-ray photoelectron spectroscopy (XPS), X-ray diffraction (XRD) and others analytical studies. $N_2$ adsorption and desorption isotherm was used to determine the specific surface areas and pore volume of the nanocomposites, respectively. The bifunctional catalytic activates (ORR/OER) are determine electricity-driven water splitting using a CHI660C electrochemical workstation (CHI660, Instrument Co., China). The details of the characterization techniques are given in the Supporting Information.

## 2. Results and Discussion

The synthesis strategy of $Co_9S_8$@NSC nanocomposites are schematically depicted in Scheme 1. The phenylthiourea-formaldehyde polymer cobalt complexes [PTF–Co(II)] were prepared using the polymeric ligand and the cobalt chloride (see the details for synthesis and characterization in the Supporting Information).[11] To prepare $Co_9S_8$@NSC nanocomposite, PTF–Co(II) is used as the source of nitrogen, sulfur, carbon and metal ion as cobalt. Pyrolysis of PTF–Co(II) at 600, 700, 800 and 900 °C temperature under He (helium) atmosphere led to the one-step formation of $Co_9S_8$@NSC-600,$Co_9S_8$@NSC-700, $Co_9S_8$@NSC-800 and $Co_9S_8$@NSC-900 nanocomposites respectively. Evolved gas analysis (TGA-FTIR-MS) during the pyrolysis of the polymer metal complexes (Figure S2, Supporting Information) revealed that the precursor, PTF–Co(II),is convert in to the most of the thermally stable moieties such as benzene rings (Figure S3, Supporting Information). It is also observed that the graphitic carbon moieties are co-doped with N and S from the phenylthiourea, accompanied by a release of gases ($CO$,$CO_2$, $NH_3$, $SO_2$ and so on).[12]

Finally, $Co_9S_8$@NSC composites are obtained after etching with 10 wt% HCl, to remove the remaining trace Co and Na

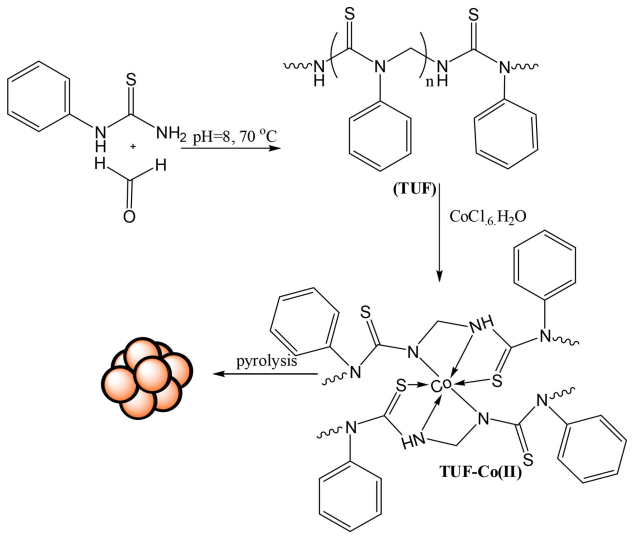


**Scheme 1.** Schematic diagram of the synthesis of $Co_9S_8$@NSC nanocomposites.

species from the product. The composition of $Co_9S_8$@NSC nanocomposites is evaluated using the elemental and ICP analysis (inductively coupled plasma) and summarized in table (Table S1, Supporting Information).The ICP-OES results confirmed the mass ratio of total Co (cobalt) in $Co_9S_8$@CNS-600, $Co_9S_8$@CNS-700, $Co_9S_8$@CNS-800 and$Co_9S_8$@CNS-900to be 9.8%, 12.42%, 13.60% and 14.78% by weight respectively.

Figure 1(a) shows the XRD pattern of $Co_9S_8$@NSC-600,$Co_9S_8$@NSC-700, $Co_9S_8$@NSC-800 and $Co_9S_8$@NSC-900 nanocomposites. The XRD patterns of the $Co_9S_8$@NSC support the presence of $Co_9S_8$ (JCPDS No. 02–1459) in the nanocomposites. The diffraction peaks at 2 $\theta = 29.8°$, 36.2°, 31.2°, 39.5°, 47.6°, and 52.0° assigned (311), (400),(100), (511) and (440) respectively, corresponding to $Co_9S_8$ phase.[13] However, all the four nanocomposites of $Co_9S_8$@NSC show the diffraction pattern of $Co_9S_8$, while increasing the temperature the intensity of $Co_9S_8$ peaks become higher, indication the crystallinity of the nanocomposites are increased. $Co_9S_8$@NSC-800 showed a broad diffraction peak around 26° and 44° corresponding to graphitic carbon. The formation of doped graphitic carbon and other thermally stable moieties were supported by FTIR spectra and thermogravimetric analysis results (Figures S4 and S5, Supporting Information).[14] As the temperature of nanocomposites preparation was increased the intensity and sharpness of diffraction peaks related to graphitic carbon were increases that support more graphitization with higher temperature and further supported with Raman spectroscopy. The Raman spectra of the prepared $Co_9S_8$@NSC nanocomposite are shown in Figure 1b. Several Raman peaks were seen at 162.5, 233.5, 341.7, 470.2, 511.1, 606.1 and 675.8 $cm^{-1}$ assigned to $Co_9S_8$.[15] Two peaks at 1342 and 1585 $cm^{-1}$ correspond to the D and G peaks of carbon materials. The intensity ratio ($I_D/I_G$) values of the nanocomposite varied with the temperature and indicate the defect level of carbon is increase with increasing temperature. In the case of $Co_9S_8$@NSC-800, the intensity ratio was

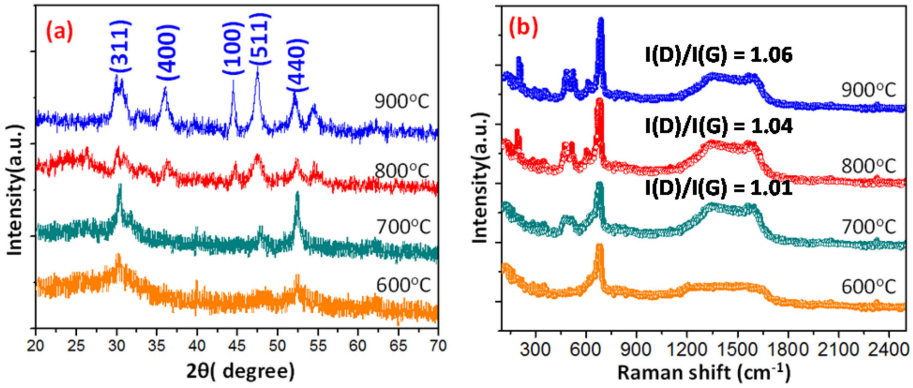


**Figure 1.** X-Ray diffraction patterns (a) and Raman spectra (b) of $Co_9S_8$@NSC nanocomposites at different pyrolysis temperatures.

found to be 1.04 and support the defective nature of graphite carbon.[16]

The essential characteristics of the surface and chemical composition as well as the valance states of the metal/metal ions were analyzed using X-ray photoelectron spectroscopy (XPS) as shown in Figure S6 (Supporting Information). Apart from cobalt, sulfur, carbon and oxygen, the presence of nitrogen was also detected in the entire nanocomposite materials. The elemental composition was found to be 78.24%, 5.18%, 3.80% and 12.54% of C, N, S, and Co, respectively, in $Co_9S_8$@NSC-800, which is close to similar that of elemental analysis results. The Co 2p core level spectra contain two sets of peaks as shown in Figure 2(a). The peaks at 779.40 and 795.61 eV are corresponding to $Co2p_{3/2}$ and the peaks at 781.20 and 796.61 eV are assigned to Co $2p_{1/2}$ and support the formation of $Co_9S_8$ in the nanocomposites.[17] The doublets are characteristic peaks of $Co^{2+}$ and $Co^{3+}$. The energy difference between Co $2p_{3/2}$ and $2p_{1/2}$ was observed to be 15 eV due to spin–orbit splitting and agree with Co 2p of $Co_9S_8$. Another peak 778.41 eV was observed and assigned to Co–S and the peak at 780.49 eV can be attributed to the Co with N in the Co–$N_x$ structure.[18]

Two satellite peaks at 781.88 eV and 797.05 eV were found corresponding to Co $2p_{3/2}$ and $2p_{1/2}$ respectively.[19]

The high-resolution spectrum of S 2p show five species of sulfur $S2p_{1/2}$, $S2p_{3/2}$, Co–S, –S=C (thiophene-like sulfur) and SOx (oxidized sulfur species) at 161.6 eV, 162.8 eV, 163.5 eV, 164.4 eV and 168.4 eV respectively.[5b,8b]. The strong SOx peaks could be

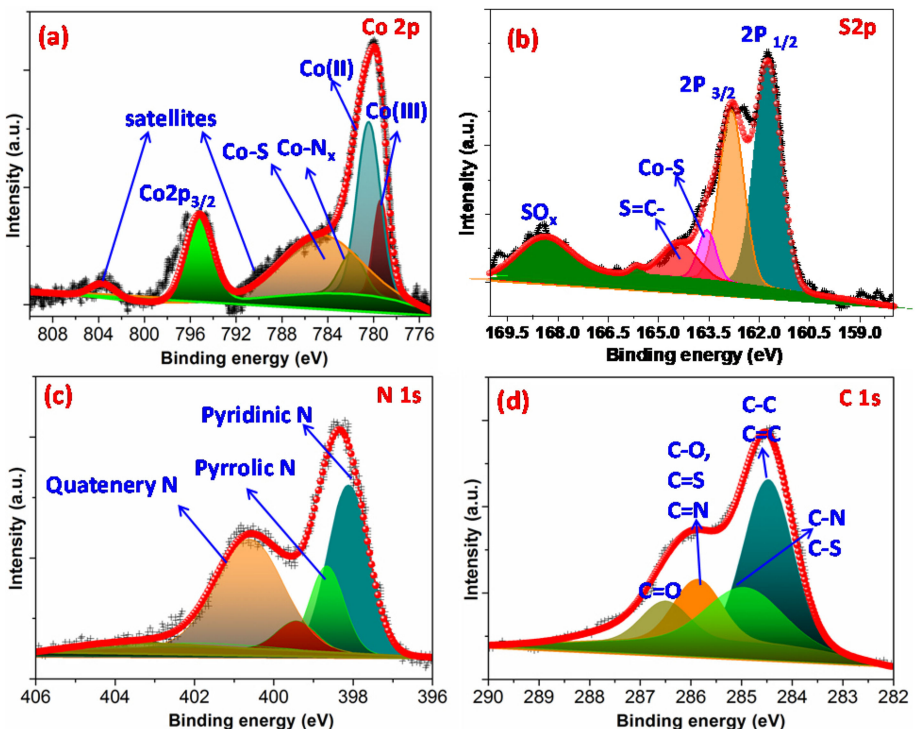


**Figure 2.** High-resolution XPS survey for $Co_9S_8$@CNS-800: Co 2p (a), C 1s (b), N 1s (c), and S 2p (d).

due to the adsorbed oxygen on the $Co_9S_8$ active surface. The high-resolution N 1s spectrum of nanocomposite is shown in Fig 2c, the N 1s peaks are split into five peaks. A very low intense peak is observed at 399.38 eV corresponding to Co–Nx species. Other peaks were also observed at 397.71 (pyridinic N), 398.50 (pyrrolic N), 400.21(graphitic/quaternary N), and 404.40 eV (N-oxides of pyridinic N) and support the present nitrogen in different species.[20] The high-resolution C 1s spectrum as shown in fig 2d, shows a strong peak at 284.2 eV assigned to the C=C formed during the graphitization of nanocomposite. The presence of C–S and C–N species in the nanocomposites are observed due to the presence of a sharp peak at 285.62 eV, indicating the formation of S and N co-doped graphite carbon and supported with FT-IR (Figure S4, Supporting Information).[15,19] Another peaks due to C=O and C–O were observed at 288.2 eV and 285.4 eV respectively. It is believed that graphite carbon with nitrogen and sulfur containing groups have better donor–acceptor properties and show excellent charge mobility in the carbon atom matrix, which will induce enhanced catalytic activity in electron-transfer reactions. $N_2$ adsorption–desorption isotherm curves $Co_9S_8$@CNS nanocomposites are presented in Figure S7 (Supporting Information) it was observed that the absorbed volumes of $N_2$ were found greater than that of the polymer metal complexes. It was also observed that the absorbed volumes of $N_2$ were increase with increasing the pyrolysis temperature of the nanocomposites. The specific surface areas and pore volumes of $Co_9S_8$@CNS nanocomposites are summarized in Table S2 (Supporting Information), the large surface area, three dimensional structure and large pore volume and pore size of mesoporous $Co_9S_8$@CNS nanocomposites support their electrocatalytic applications.[21]

The morphology of $Co_9S_8$@CNS nanocomposites prepared at 600, 700, 800 °C and 900 °C shown in Figure S8 (Supporting Information). The TEM image of $C_9S_8$@CNS-600 revealed that the nanoparticles grown in the carbon matrix with an irregular particles size of about 10–42 nm; on the other hand, $Co_9S_8$@CNS-700, some nanoparticles of $Co_9S_8$ was observed on the surface of graphite carbons and an average particle size was found to be ~67 nm. $Co_9S_8$@CNS-800 exhibits narrow spherical particle size distribution compared to that of other nanocomposites, and the average particles size was observed about 81 nm and distributed uniformly on the surface of the porous graphite carbon. The detailed morphology of the $Co_9S_8$@CNS nanocomposites was investigated by TEM and HRTEM. Figure 3a shows that the spherical nanoparticles of $Co_9S_8$@CNS-800 are uniform in both, size and shape, and also well encapsulated in the graphite carbon. The HRTEM image of the $Co_9S_8$@CNS-800 is shown in Figure 3(b), it was observed that the size of $Co_9S_8$ nanoparticles was about 10 nm and the d-spacing value (lattice fringes) was found to be 0.29 nm assigned to the (311) plane of $Co_9S_8$.[22] It is clearly observed that the $Co_9S_8$nanoparticle was wrapped inside graphite carbon layers.

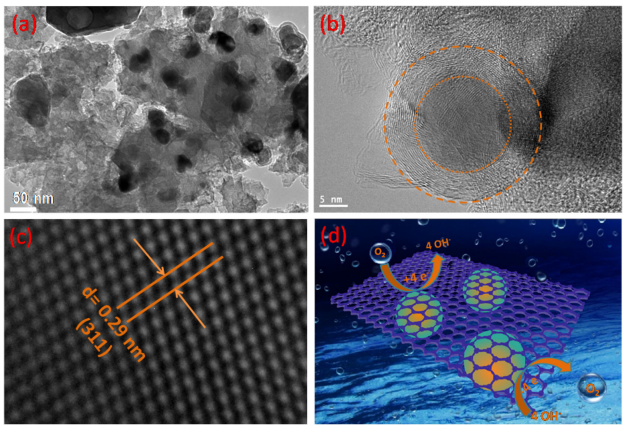


**Figure 3.** TEM image of $Co_9S_8$@CNS-800 (a), HRTEM image of $Co_9S_8$@CNS-800 (b), spacing representation (c), and schematic diagram for ORR (d).

## 3. Electrocatalyst Activity and Stability

The ORR electrocatalytic activities of $Co_9S_8$@NSC nanocomposites are accomplished via three-electrode system. The observed potentials were calibrated with reference to the reversible hydrogen electrode (RHE) for comparison purposes (the calibration is given in the Supporting Information). Cyclic voltammetry (CV) curves of prepared nanocomposites illustrate cathodic peaks in $O_2$-saturated 0.1 M KOH solution at 0.625 V ($Co_9S_8$@NSC-600), 0.646 V ($Co_9S_8$@NSC-700), 0.867 V ($Co_9S_8$@NSC-800) and 0.726 V ($Co_9S_8$@NSC-900). However, no redox peaks were observed with $N_2$-saturated 0.1 M KOH solution. All the prepared $Co_9S_8$@NSC nanocomposites exhibit excellent catalytic activity in alkaline medium. It was observed that the ORR peak was shifted towards positive potentials when the reaction temperature was increased from 600 to 800 °C indicating the outstanding ORR, but after further increasing the temperature up to 900 °C the catalytic activities decreased as shown in Figure S9 (Supporting Information). This is because, when the temperature of the carbonization was increased, the degree of graphitization was also increased which leads the electric conductivity of the $Co_9S_8$@NSC nanocomposite.[9c,23]

On the other hand, overheating of the nanocomposites reduced or decomposed the dopants and hence reduction potential was decreased from $Co_9S_8$@NSC-800 to $Co_9S_8$@NSC-900.

The linear sweep voltammetry (LSV) curves of $Co_9S_8$@NSC nanocomposites are shown in Figure 4 (b). The onset potential ($E_o$) was observed 0.851 V ($Co_9S_8$@NSC-600), to 0.892 V ($Co_9S_8$@NSC-700) and 0.976 V ($Co_9S_8$@NSC-800). Evidently, the catalytic activities during ORR were increased in order of $Co_9S_8$@NSC-600 < $Co_9S_8$@NSC-700 < $Co_9S_8$@NSC-800 > $Co_9S_8$@NSC-900, in good in agreement with the cyclic voltammetry results, indicating the excellent electrocatalytic activity for the ORR.

The $Co_9S_8$@NSC-800 shows an excellent onset potential ($E_o$) and half-wave potential ($E_{1/2}$) of 0.976 and 0.865 V, respectively, on the other hand the commercial Pt/C (20%) shows the $E_o$ and

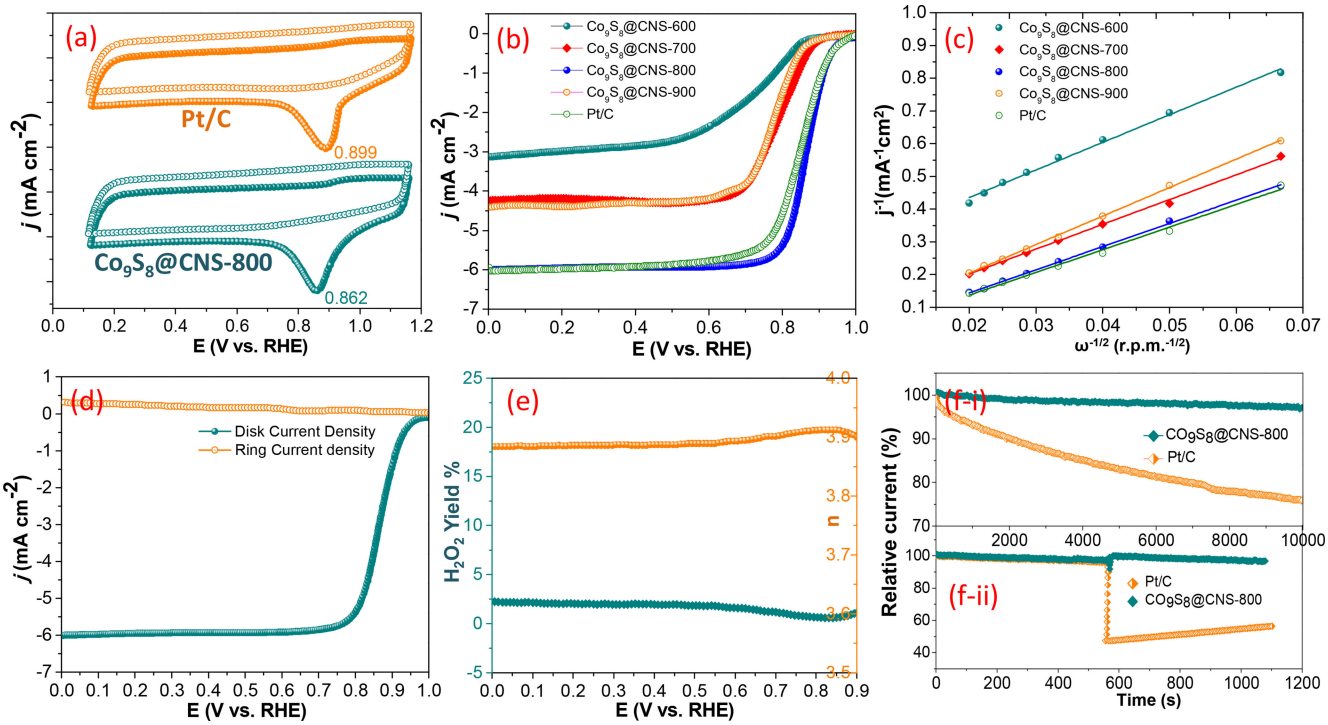


**Figure 4.** CV of Pt/C and $Co_9S_8$@NSC-800 at a scan rate of 50 mV s$^{-1}$ in $N_2$- and $O_2$-saturated 0.1 M KOH aqueous solution (vacant in $N_2$ and field in $O_2$) (a), LSV curves at a scan rate of 10 mV s$^{-1}$ at a rotational speed of 1600 rpm (b), K–L plots of nanocomposites at different potentials from 0.2.5 to 0.7.5 V (c), the ring current and disk current on a $Co_9S_8$@NSC-800 electrode at 1600 rpm at a scan rate of 10 mV s$^{-1}$(d), $H_2O_2$ yields and number of electron transfer during ORR (e), and the durability (f-I) and methanol crossover effect test (f-II) of Co9S8/NSC-800 and Pt/C.

the $E_{1/2}$ potential 1.00 and 0.850 V respectively and shown better results when compared with previously reported catalysts (Table S2, Supporting Information)..[24] The kinetics and catalytic mechanism during the ORR, were further carried out using LSV tests with different rotating rates (225 ~ 2500 rpm) and the results are illustrated in Figures (Supporting Figures 13–14). Koutecky–Levich (K–L) equation was used to determine the kinetic parameters and the numbers of electrons transfer per molecules of oxygen (see the Supporting Information). All the nanocomposites show good linearity and the nearly parallel fitted lines between $j^{-1}$ and $\omega^{-1/2}$ of the K–L plots illustrates the first-order reaction for ORR and the number of electrons (*n*) is calculated between 0.0–0.90 V and found to be 3.87–3.93, which indicates that it favors a 4*e*$^-$ oxygen reduction process as shown in Figure 4c, about to 4.00 (the theoretical value for commercial Pt/C).[8c,25] The lower Tafel slopes observed for $Co_9S_8$@NSC-800 catalysts suggest the better ORR activity (Figure S15, Supporting Information). To further understand the electron transfer pathway and to monitor the peroxide ($H_2O_2$) yield an undesired byproduct from ORR[26] rotating ring-disk electrode (RRDE) measurements are carried out as shown in Figures 4d–4e. Remarkably, the $H_2O_2$ yield of $Co_9S_8$@NSC-800 is below 1.9% in the potential range investigated, and the number of electrons transfer (n) was found to be 3.95, which is consistent with the results on the RDE data.[27] The chronoamperometric response of $Co_9S_8$@NSC-800 and the commercial Pt/C catalysts were carried out in 0.1 M KOH solution ($O_2$-saturated) with a rotation rate of 1,600 rpm at 0.6Vfor 10,000 s (Figure 4f-I). The results revealed that in the case of $Co_9S_8$@NSC-800, around 96% of the current was maintained while; in the case of Pt/C, 29% loss of current density was observed. In addition, the fuel crossover effect and durability of the catalyst are serious concern for water splitting. During the fuel crossover effect, 3 M methanol was added after the test had run 560 s, the direction of current response reverses immediately after adding methanol. The phenomenon indicates the occurrence of methanol electro-oxidation under this potential. These results suggest that $Co_9S_8$@NSC-800 exhibits excellent tolerance to methanol and superior selectivity for oxygen reduction reaction then Pt/C.[5b,28] Additionally, $Co_9S_8$@NSC-800 exhibits excellent durability for ORR in alkaline condition as shown in Figure 4d.

Oxygen evaluation reaction (OER) activities of the $Co_9S_8$@NSC-800 and the standard commercial catalyst $RuO_2$ were also characterized in 0.1 M KOH system as described in the Experimental Section (see also the Supporting Information). Figure 5a shows the polarization curves of $Co_9S_8$@NSC nanocomposites and $RuO_2$ electrocatalyst obtained at a scan rate of 5 mV s$^{-1}$. An obvious rise of the anodic current at an onset potential of ~1.54 V (vs. RHE) was observed for the $Co_9S_8$@NSC-800. This was ~6 mV far that of $RuO_2$, indicating the superior intrinsic catalytic activity of the $Co_9S_8$@NSC catalyst towards OER.[29] These values are apparently higher than those of other$Co_9S_8$@NSC in this study, and also higher than the most of the commonly reported carbon based electrocatalysts (see Table S3, Supporting Information, for further comparison). The

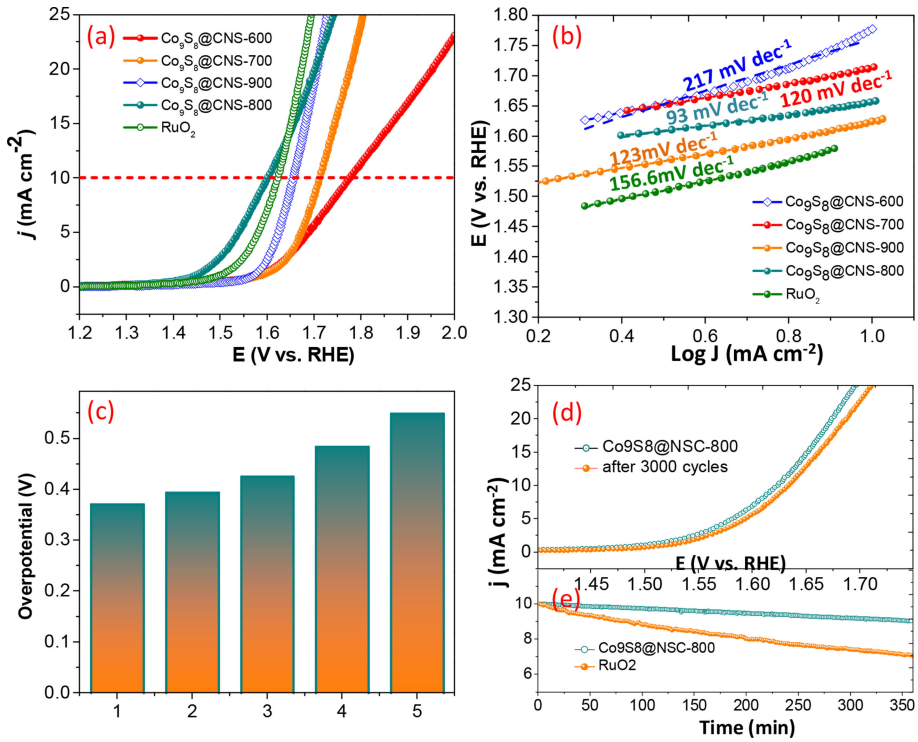


**Figure 5.** Polarization curve (iR-corrected) for OER at 1600 rpm at a scan rate of 10 mV $s^{-1}$ (a). Corresponding OER Tafel plots (b). The required overpotential to achieve a current density of 10 mA $cm^{-2}$ for different electrocatalysts (c). Stability of the $Co_9S_8$@NSC-800 catalyst after 3000 cycles (d). The durability test of $Co_9S_8$@NSC-800 and $RuO_2$ in O2-saturated 0.1 M KOH at 1.53 (e).

Key parameter for OER (potential required at a current density of 10 mA $cm^{-2}$, $\eta_{10}$) is used to judge the catalytic activities of $Co_9S_8$@NSC nanocomposites and compare with $RuO_2$.[30]

It has been seen that, the $Co_9S_8$@NSC-800 catalyst show the over-potential 391 mV (compared with the standard reaction potential) at $\eta_{10}$, while the $Co_9S_8$@NSC-600, $Co_9S_8$@NSC-700 and $Co_9S_8$@NSC-900 show 549 mV, 483 mV, and 549 mV over-potential respectively as shown in Figure 4c.The over-potential value of the $Co_9S_8$@NSC-800 is lower than the other $Co_9S_8$@NSC nanocomposites and close to that of the commercial $RuO_2$ catalyst and leads the superior catalytic activity for OER in basic medium (Figure 5a).

In addition, the OER kinetics of $Co_9S_8$@NSC nanocomposites are studied by plotting their Tafel curves, as shown in Figure 5b. The resulting Tafel slopes are found to be 217, 120, 93, 123 and 156.6 mV $dec^{-1}$ for $Co_9S_8$@NSC-600, $Co_9S_8$@NSC-700, $Co_9S_8$@NSC-900 and $Co_9S_8$@NSC-800, and the commercial $RuO_2$, respectively. Although all nanocomposites exhibit ORR, however the lower Tafel plot value is observed between (1.45 to 1.80 V) suggests that the $Co_9S_8$@NSC-800 the most efficient OER catalyst among all the samples in this study.

The results of stability test during ORR revealed that the $Co_9S_8$@NSC-800 is very stable catalyst (Figure 5d and5e), whereas the durability during the ORR was observed between 0.2 to 1.0 V with 50 mV $s^{-1}$ scan rate up to 3000 cycles and exhibits excellent results compare to the commercial $RuO_2$. These results proposed that the $Co_9S_8$@NSC-800 nanocomposite is an efficient electrocatalyst for ORR and OER.

## 4. Conclusions

We have successfully developed low-cost materials; $Co_9S_8$ nanocrystals encapsulated in nitrogen/sulfur doped mesoporous graphitized carbon, simply by pyrolyzing polymer metal complex. This is the first time that a polymer metal complex has been utilized as single source to synthesize the nanocomposites containing sulfur, nitrogen, carbon, and $Co_9S_8$. It was observed that catalytic activity of nanocomposites was increased with their preparation temperature from 600 to 800 °C, but after further increasing the preparation temperature up to 900 °C and more the catalytic activities decreased because overheating reduced or decomposed the dopants. The resultants nanocomposites exhibit remarkable catalytic activities for both ORR and OER with high current densities, low onset potentials, and excellent stability and even outperform a commercial Pt/C and $RuO_2$ electrocatalyst as a bifunctional electrocatalyst. We anticipate that our nanomaterials will also be useful for other electrocatalytic applications.

## *Acknowledgement*

*The authors extend their sincere appreciation to the Deanship of Scientific Research at King Saud University for funding this Research Group (RG-1438-026).*

## Conflict of Interest

The authors declare no conflict of interest.

**Keywords:** electrocatalysts · nanocrystals · carbon · oxygen evolution reactions

[1] a) J. Y. Jia, L. C. Seitz, J. D. Benck, Y. J. Huo, Y. S. Chen, J. W. D. Ng, T. Bilir, J. S. Harris, T. F. Jaramillo, *Nat. Commun.* **2016**, *7*; b) Q. Wang, T. Hisatomi, Q. X. Jia, H. Tokudome, M. Zhong, C. Z. Wang, Z. H. Pan, T. Takata, M. Nakabayashi, N. Shibata, Y. B. Li, I. D. Sharp, A. Kudo, T. Yamada, K. Domen, *Nat. Mater.* **2016**, *15*, 611-+; c) G. Li, X. L. Wang, J. Fu, J. D. Li, M. G. Park, Y. N. Zhang, G. Lui, Z. W. Chen, *Angew. Chem. Int. Ed.* **2016**, *55*, 4977–4982; d) J. B. Zhu, M. L. Xiao, Y. L. Zhang, Z. Jin, Z. Q. Peng, C. P. Liu, S. L. Chen, J. J. Ge, W. Xing, *ACS Catal.* **2016**, *6*, 6335–6342; e) J. W. D. Ng, M. Tang, T. F. Jaramillo, *Energ. Environ. Sci.* **2014**, *7*, 2017–2024; f) M. D. Radin, D. J. Siegel, *Energ. Environ. Sci.* **2013**, *6*, 2370–2379.

[2] a) Z. C. Zhang, Z. M. Luo, B. Chen, C. Wei, L. Zhao, J. Z. Chen, X. Zhang, Z. C. Lai, Z. X. Fan, C. L. Tan, M. T. Zhao, Q. P. Lu, B. Li, Y. Zong, C. C. Yan, G. X. Wang, Z. J. C. Xu, H. Zhang, *Adv. Mater.* **2016**, *28*, 8712–8717; b) A. Sivanantham, P. Ganesan, S. Shanmugam, *Adv. Funct. Mater.* **2016**, *26*, 4661–4672.

[3] a) T. Bhowmik, M. K. Kundu, S. Barman, *ACS Appl. Mater. Interfaces* **2016**, *8*, 28678–28688; b) M. Roca-Ayats, E. Herreros, G. Garcia, M. A. Pena, M. V. Martinez-Huerta, *Appl. Catal. B-Environ* **2016**, *183*, 53–60; c) M. D. Obradovic, U. C. Lacnjevac, B. M. Babic, P. Ercius, V. R. Radmilovic, N. V. Krstajic, S. L. Gojkovic, *Appl. Catal. B-Environ* **2015**, *170*, 144–152; d) J. Ahmed, Y. Mao, *Electrochim. Acta* **2016**, *212*, 686–693.

[4] a) S. Dresp, F. Luo, R. Schmack, S. Kuhl, M. Gliech, P. Strasser, *Energ. Environ. Sci.* **2016**, *9*, 2020–2024; b) J. J. Duan, S. Chen, A. Vasileff, S. Z. Qiao, *ACS Nano* **2016**, *10*, 8738–8745; c) S. Dong, X. Chen, X. Zhang, G. Cui, *Coord. Chem. Rev.* **2013**, *257*, 1946–1956; d) Z. Zhang, X. Wang, G. Cui, A. Zhang, X. Zhou, H. Xu, L. Gu, *Nanoscale* **2014**, *6*, 3540–3544.

[5] a) X. Y. Li, Z. G. Niu, J. Jiang, L. H. Ai, *J. Mater. Chem. A* **2016**, *4*, 3204–3209; b) P. Ganesan, M. Prabu, J. Sanetuntikul, S. Shanmugam, *ACS Catal.* **2015**, *5*, 3625–3637; c) J. Masud, A. T. Swesi, W. P. R. Liyanage, M. Nath, *ACS Appl. Mater. Interfaces* **2016**, *8*, 17292–17302.

[6] T. Yoon, K. S. Kim, *Adv. Funct. Mater.* **2016**, *26*, 7386–7393.

[7] a) L. L. Feng, M. H. Fan, Y. Y. Wu, Y. P. Liu, G. D. Li, H. Chen, W. Chen, D. J. Wang, X. X. Zou, *J. Mater. Chem. A* **2016**, *4*, 6860–6867; b) J. M. Falkowski, Y. Surendranath, *ACS Catal.* **2015**, *5*, 3411–3416.

[8] a) S. Dou, L. Tao, J. Huo, S. Y. Wang, L. M. Dai, *Energ. Environ. Sci.* **2016**, *9*, 1320–1326; b) H. Hu, L. Han, M. Z. Yu, Z. Y. Wang, X. W. Lou, *Energ. Environ. Sci.* **2016**, *9*, 107–111; c) H. X. Zhong, K. Li, Q. Zhang, J. Wang, F. L. Meng, Z. J. Wu, J. M. Yan, X. B. Zhang, *NPG Asia Mater.* **2016**, *8*; d) J. Yang, G. X. Zhu, Y. J. Liu, J. X. Xia, Z. Y. Ji, X. P. Shen, S. K. Wu, *Adv. Funct. Mater.* **2016**, *26*, 4712–4721.

[9] a) G. Wu, N. H. Mack, W. Gao, S. G. Ma, R. Q. Zhong, J. T. Han, J. K. Baldwin, P. Zelenay, *ACS Nano* **2012**, *6*, 9764–9776; b) S. Dou, L. Tao, J. Huo, S. Wang, L. Dai, *Energy and Environmental Science* **2016**, *9*, 1320–1326; c) H. Hu, L. Han, M. Yu, Z. Wang, X. W. Lou, *Energy and Environmental Science* **2016**, *9*, 107–111.

[10] T. Ahamad, S. M. Alshehri, *Spectrochim Acta A* **2013**, *108*, 26–31.

[11] S. Parveen, T. Ahamad, N. Nishat, *Appl. Organomet. Chem.* **2008**, *22*, 70–77.

[12] T. Ahamad, S. M. Alshehri, *J. Therm. Anal. Calorim.* **2012**, *109*, 1039–1047.

[13] a) Y. C. Chen, Y. G. Zhang, *Spectrosc. Spect. Anal.* **2006**, *26*, 1117–1119; b) S. Álvarez-Torrellas, M. Martin-Martinez, H. T. Gomes, G. Ovejero, J. García, *Appl. Surf. Sci.* **2017**, *414*, 424–434; c) B. Hu, Z. Jing, J. Fan, G. Yao, F. Jin, *Catal. Today* **2016**, *263*, 128–135.

[14] M. Naushad, T. Ahamad, B. M. Al-Maswari, A. Abdullah Alqadami, S. M. Alshehri, *Chem. Eng. J.* **2017**, *330*, 1351–1360.

[15] R. Li, Y. Dai, B. B. Chen, J. L. Zou, B. J. Jiang, H. G. Fu, *J. Power Sources* **2016**, *307*, 1–10.

[16] L. L. Feng, G. D. Li, Y. P. Liu, Y. Y. Wu, H. Chen, Y. Wang, Y. C. Zou, D. J. Wang, X. X. Zou, *ACS Appl. Mater. Interfaces* **2015**, *7*, 980–988.

[17] Q. M. Su, G. H. Du, J. Zhang, Y. J. Zhong, B. S. Xu, Y. H. Yang, S. Neupane, K. Kadel, W. Z. Li, *ACS Nano* **2013**, *7*, 11379–11387.

[18] K. Niu, B. Yang, J. Cui, J. Jin, X. Fu, Q. Zhao, J. Zhang, *J. Power Sources* **2013**, *243*, 65–71.

[19] J. Mujtaba, H. Y. Sun, G. Y. Huang, Y. Y. Zhao, H. Arandiyan, G. X. Sun, S. M. Xu, J. Zhu, *RSC Adv.* **2016**, *6*, 31775–31781.

[20] H. Zhang, Y. Wang, D. Wang, Y. Li, X. Liu, P. Liu, H. Yang, T. An, Z. Tang, H. Zhao, *Small* **2014**, *10*, 3371–3378.

[21] a) B. Chen, R. Li, G. Ma, X. Gou, Y. Zhu, Y. Xia, *Nanoscale* **2015**, *7*, 20674–20684; b) Z. Wang, X. Cao, J. Ping, Y. Wang, T. Lin, X. Huang, Q. Ma, F. Wang, C. He, H. Zhang, *Nanoscale* **2015**, *7*, 9394–9398.

[22] R. Li, Y. Dai, B. Chen, J. Zou, B. Jiang, H. Fu, *J. Power Sources* **2016**, *307*, 1–10.

[23] a) H. X. Zhong, J. Wang, Y. W. Zhang, W. L. Xu, W. Xing, D. Xu, Y. F. Zhang, X. B. Zhang, *Angewandte Chemie – International Edition* **2014**, *53*, 14235–14239; b) X. Zou, X. Huang, A. Goswami, R. Silva, B. R. Sathe, E. Mikmeková, T. Asefa, *Angew. Chem.* **2014**, *126*, 4461–4465.

[24] a) J. C. Li, P. X. Hou, S. Y. Zhao, C. Liu, D. M. Tang, M. Cheng, F. Zhang, H. M. Cheng, *Energ. Environ. Sci.* **2016**, *9*, 3079–3084; b) S. Gadipelli, T. T. Zhao, S. A. Shevlin, Z. X. Guo, *Energ. Environ. Sci.* **2016**, *9*, 1661–1667.

[25] a) R. Gao, Z. Y. Li, X. L. Zhang, J. C. Zhang, Z. B. Hu, X. F. Liu, *ACS Catal.* **2016**, *6*, 400–406; b) J. Wang, Z. X. Wu, L. L. Han, R. Q. Lin, H. L. L. Xin, D. L. Wang, *ChemCatChem* **2016**, *8*, 736–742.

[26] H. Li, H. Liu, Z. Jong, W. Qu, D. S. Geng, X. L. Sun, H. J. Wang, *Int. J. Hydrogen Energy* **2011**, *36*, 2258–2265.

[27] a) T. Maiyalagan, K. A. Jarvis, S. Therese, P. J. Ferreira, A. Manthiram, *Nat. Commun.* **2014**, *5*; b) J. T. Zhang, Z. H. Zhao, Z. H. Xia, L. M. Dai, *Nat. Nanotechnol.* **2015**, *10*, 444–452.

[28] a) Y. P. Zhu, Y. P. Liu, T. Z. Ren, Z. Y. Yuan, *Adv. Funct. Mater.* **2015**, *25*, 7337–7347; b) J. W. Xiao, C. Chen, J. B. Xi, Y. Y. Xu, F. Xiao, S. Wang, S. H. Yang, *Nanoscale* **2015**, *7*, 7056–7064.

[29] a) Z. J. Jiang, Z. Q. Jiang, *Sci. Rep.* **2016**, *6*; b) G. L. Tian, M. Q. Zhao, D. S. Yu, X. Y. Kong, J. Q. Huang, Q. Zhang, F. Wei, *Small* **2014**, *10*, 2251–2259.

[30] a) F. L. Yang, P. P. Zhao, X. Hua, W. Luo, G. Z. Cheng, W. Xing, S. L. Chen, *J. Mater. Chem. A* **2016**, *4*, 16057–16063; b) X. J. Xu, P. Y. Du, Z. K. Chen, M. H. Huang, *J. Mater. Chem. A* **2016**, *4*, 10933–10939.

Manuscript received: September 12, 2017
Version of record online: ■■ ■■, 0000

# ARTICLES

**Time to split:** The synthesis of $Co_9S_8$ nanocrystals encapsulated in nitrogen/sulfur-doped mesoporous graphitized carbon derived from a polymer–metal complex is reported. The nanocrystals exhibit similar electrocatalytic activity and superior stability for water-splitting reactions (oxygen reduction/oxygen evolution). The remarkable electrochemical properties are mainly attributed to the synergetic effects between $Co_9S_8$, heteroatoms, and graphitized carbon in alkaline medium, especially for the oxygen evolution reaction.